Defence Science Journal, Vol. 73, No. 2, March 2023, pp. 220-230, DOI : 10.14429/dsj.73.18719
© 2023, DESIDOC

Realization of High Pressure Turbine Blades of a Small Turbo-Fan Engine through Investment Casting Process

D. Chatterjee[#], A.S. Chauhan[#] , Venkat[#], D.P. Tigga[$] and D.K. Das[#,*]

[#]*DRDO-Defence Metallurgical Research Laboratory, Kanchanbagh, Hyderabad - 500 058, India*
[$]*DRDO-Gas Turbine Research Establishment, CV Raman Nagar, Bengaluru – 560 093, India*
[*]*E-mail: dkdas.dmrl@gov.in*

ABSTRACT

Turbo-fan gas turbine engines, or simply turbo-fan engines (STFEs), are used for powering both manned aircrafts and unmanned air vehicles (UAVs). The high pressure turbine section of such engines use Ni-base superalloy cast rotor blades because of their good mechanical properties at high operating temperatures. The present paper provides the technical/technological details of the various aspects associated with development and manufacturing of high pressure turbine blades (HPTBs) for utilization in an indigenously-developed small turbo-fan engine. Vacuum investment casting process has been adopted for realization of the above equiaxed components using a Ni-base superalloy.

Keywords: Gas turbine blade; Superalloy; Investment casting; Microstructure; Mechanical property

1. INTRODUCTION

An expendable small turbo-fan engine (STFE) having a twin spool configuration has been developed by DRDO for meeting the propulsion needs of a certain class of unmanned air vehicles (UAVs). This engine contains a single-stage high pressure (HP) turbine which consists of one stator and one rotor. The rotor, in turn, comprises fifty solid un-shrouded blades, also called as high pressure turbine blades (HPTBs), individually cast, machined and assembled on a forged disk.

High pressure turbine blades are used in the turbine section of a gas turbine engine and they are responsible for extracting energy from the high temperature-high pressure gases produced by the combustor. The typical size of an HPTB varies from 5 cm in small gas turbines to about 150 cm in land-based gas turbines. These turbine blades operate in aggressive environments involving high mechanical stresses, elevated temperatures and corrosive/oxidative gases[1-2]. Because of their excellent high temperature properties, cast Ni-base superalloys have been traditionally used in the hot sections of turbines of both aero and industrial gas turbine engines.

Over the years, for catering to the ever increasing requirement of high turbine entry temperature (TET), wrought Ni-base superalloys have given way to cast versions which have much higher temperature capabilities. In case of cast components, use of internally cooled (i.e., hollow) ones (as opposed to solid ones) has also led to further increase in TET. Adoption of directionally solidified (DS) and single crystal components over equiaxed ones has also raised the temperature capability of superalloy parts[3-4].

Received : 21 November 2022, Revised : 20 December 2022
Accepted : 02 February 2023, Online published : 06 April 2023

In the present paper, the various aspects involved in manufacturing of equiaxed HPT blades of the above mentioned (DRDO-developed) turbo-fan engine through vacuum investment casting method have been provided. A commercially available Ni-base superalloy has been used for realizing the blades.

2. COMPONENT DESCRIPTION

Figure 1 presents the photograph of an HPT blade under consideration. It has approximate length of 40 mm, maximum width (in the platform region) of 30 mm and maximum thickness (in platform region) of 12 mm. This is a much smaller blade than its counterparts used in larger engines where the corresponding dimensions would be approximately 90, 60 and 25 mm, respectively. The various dimensions defining the aerofoil of the blade, namely R_1, R_2, T_{max}, C and α, at three cross-sections of the aerofoil, namely AB, AC and AD are provided (Fig. 2 (a)).

A typical cross-section of the aerofoil showing these dimensions is presented in Fig. 2(b). R_1 and R_2 refer to the radius of curvature at LE and TE, respectively. C in the above figure indicates the chord length, T_{max} the maximum diameter of the inscribed circle and α angle between the chord line and plane PD. It may be mentioned that the stacking axis, as shown in Fig. 2(b), is an imaginary line that is perpendicular to engine axis and all the airfoil sections are defined along this axis (i.e. stacking axis).The actual dimensions in all three sections are mentioned in Table1. The various tolerances for the component are provided in Table 2. A commercially available Ni-base superalloy having a nominal composition (wt.%) of Ni-4.5Ti-5.5Al-0.7V-0.7Nb-3.0Mo-1.4W-13.5Co-9.5Cr-0.15C, has been used for this component.

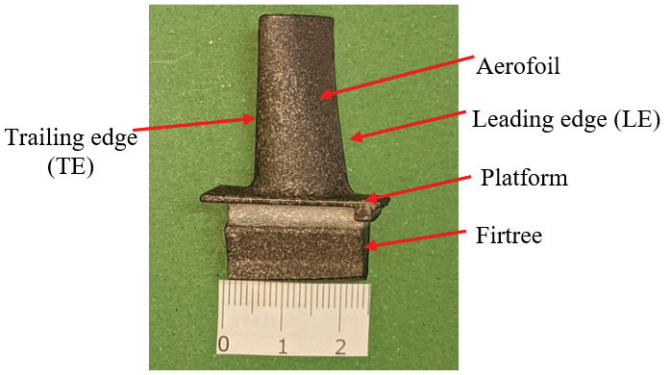

Figure 1. The photograph of an HPT blade showing its various regions.

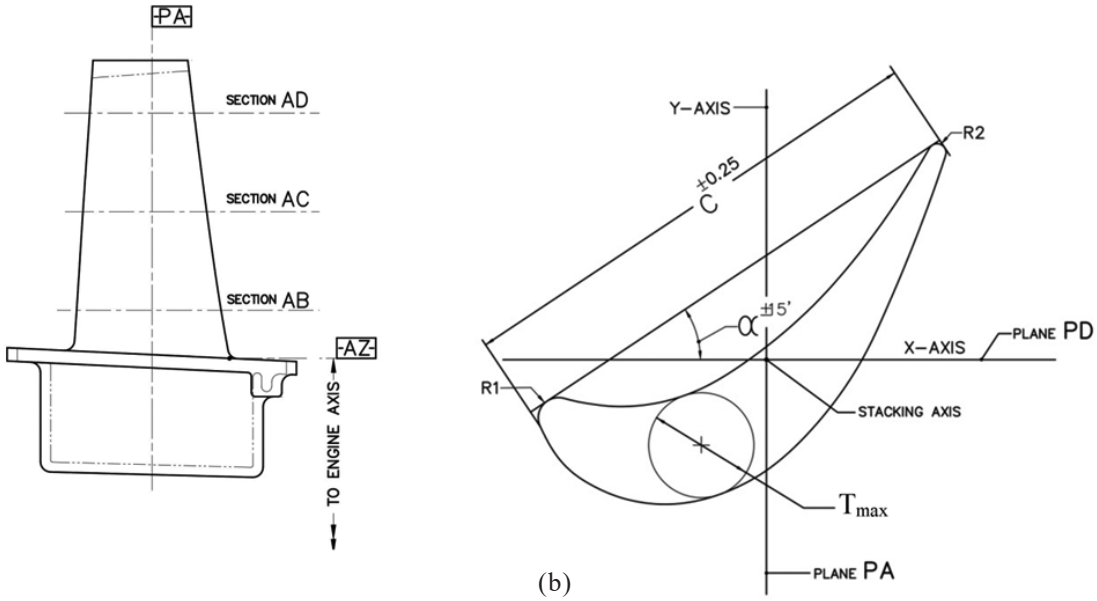

(a) (b)

Figure 2. (a) Schematic of a HPT blade showing the three sections AB, AC and AD and (b) typical aerofoil cross-section of the blade.

Table 1. Various dimensions in AB, AC and AD sections of the blade (see Fig. 2), as provided by the user agency

Section	AB	AC	AD
R_1 (mm)	0.8	0.6	0.6
R_2 (mm)	0.3	0.3	0.3
T_{max} (mm)	4.3	3.2	2.5
C (mm)	15.5	14.5	15.0
α	22°	33°	46°36'

Table 2. Specified tolerance values for various features of the component. TE refers to 'trailing edge' of the HPT blade

Feature/Property	Tolerance
Aerofoil Contour/Form	±0.13 mm
Profile (Stacking axis) displacement	X: ±0.3 mm Y: ±0.3 mm θ: ±0°30'
Chord Length, C	±0.25 mm
α	±0°15'

3. MANUFACTURING PROCESS DETAILS

The development and manufacturing of this component was carried out through vacuum investment casting method which is the typical method used for producing aeronautical-grade superalloy cast parts. This method of realizing aeronautical-grade cast parts has been widely reported[5-6]. The various steps involved in vacuum investment casting of the present component are indicated in Fig. 3 and details of each of these steps are provided as follows.

3.1 Die/tooling for Wax Pattern

For designing the die required for making wax pattern of the component, several of its aspects had to be considered. Firstly, the present blade is very short and has a thin and highly twisted aerofoil (Fig. 2). Further, apart from having very small radii at aerofoil trailing and leading edges, the component also has a small fillet radius between the platform (i.e. the part that joins the fir-tree with the aerofoil) and the aerofoil. Secondly, the presence of a radial feature in the platform of the blade dictates that the wax pattern die has a hinge-type construction. This would prevent breakage of the platform (of the wax pattern) during opening of the die after wax injection process. Thirdly, the values of R_1 and R_2, along with those for the T_{max} are extremely small (Table 1), especially considering the fact that the overall component dimensions are also very small (Fig. 2).While the value of R_2 is as low as 0.3 mm, the lowest values of R_1 and T_{max} are 0.55 and~2.5 mm, respectively. Further, the required tolerance values (Table 2), especially for aerofoil profile contour/form (±0.13 mm), profile displacement along stacking axis (X and Y: ±0.3 mm) and twist (θ: ± 0.5°) are particularly stringent. Such low values for dimensions and tolerance levels in the present HPT blade casting made the design and manufacturing of the wax pattern die extremely challenging. Further, issues pertaining to the filling of liquid wax in the thin aerofoil regions of the blade can be expected due to rapid cooling of wax in these regions during injection. Therefore, proper gating design assumes high importance. The

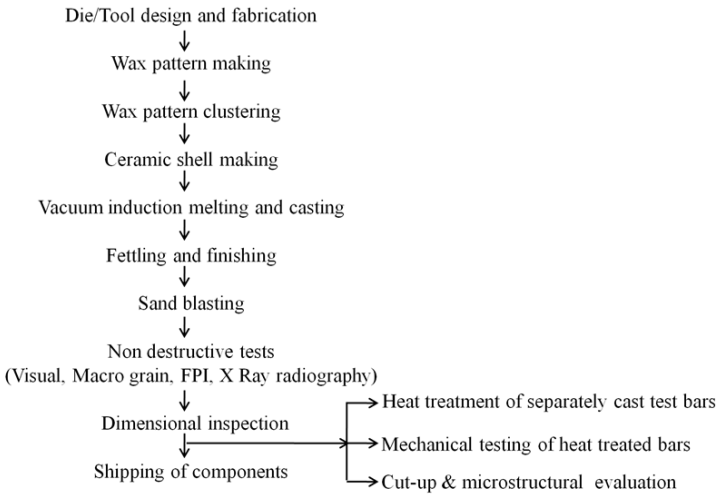

Figure 3. Flowchart of the vacuum investment casting process for realizing the present component.

last aspect pertains to manufacturing of die inserts. Typically CNC machining is adopted for manufacturing die inserts. However, the inserts which cannot be done through this route, especially at the LE/TE radii regions, EDM (electro-discharge machining) sinking method is used. Based on the above considerations, the die required for injection of wax patterns of the component was designed and manufactured, as mentioned below.

Dimensions of the wax pattern differ from those of the actual casting in two ways. The dimensions of the pattern are arrived by applying the compensation for shrinkage that occurs in the solidified casting as it cools from solidus temperature to room temperature. This shrinkage is typically anisotropic in nature (i.e. shrinkage is different in X, Y and Z directions) and needs to be appropriately compensated in the wax pattern die. An additional compensation must also be provided in the pattern dimensions to account for wax shrinkage associated with its cooling from liquid state to solid inside the pattern die after injection. For the present equiaxed blade, a total shrinkage (casting shrinkage plus wax shrinkage) compensation of 2.5% was considered for die design. Since the present HPT blade is very small in size, this shrinkage value was uniformly applied in X, Y and Z directions with reference to the stacking axis of the engine.

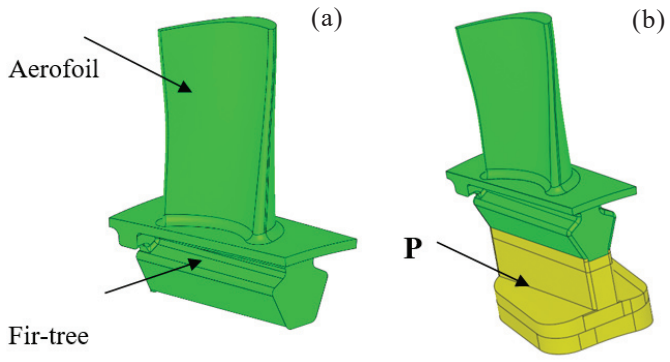

Figure 4. CAD model of (a) HPT blade made based on the castingdrawing provided by the user and (b) the corresponding wax pattern designed for die making purpose. The 'T' shaped projection at the bottom, shown as P in Fig. 4(b), was provided for easy ejection of the pattern from the die cavity.

The CAD model of the HPT blade (built based on the casting drawing) along with that of the corresponding wax pattern (designed for die making purpose)is presented in Fig. 4. A 'T'-shaped projection (marked as P in Fig. 4(b)) was deliberately added to the fir-tree portion. This additional projection not only helped in retaining the pattern in the stationary half of the pattern die but also aided in easy removal of the pattern from the die. Gating design for the wax pattern die was optimised using the wax injection simulation software Moldex3D®[7-8]. The pattern die, which had a hinged design, was divided into a number of inserts from the considerations of ease of manufacture, assembly and opening.

The inserts forming the die cavity were made from easily machinable ASTM P20 die steel and their surfaces forming the die cavity were polished to a high degree of finish (R_a value of 0.2-0.5 µm). Die inserts were machined by a suitable 3-axis CNC milling process. The small radii at LE and TE were created through EDM sinking method by using specially prepared electrodes. A 3-axis tactile coordinate measuring machine (CMM) was utilized for dimensional inspection and qualification of each die insert. After assembly, the two die halves were separately inspected with the CMM for critical dimensions with reference to the hinge and this represents the engine axis of the gas turbine. Subsequently, the fabricated die was utilized to inject actual wax patterns which were then examined for dimensional conformity.

3.2 Investment Casting Process

The vacuum investment casting method adopted for the component consists of several steps, as indicated in the flowchart shown in Fig. 3.

3.2.1 Preparation of Ceramic Mould

Wax patterns were made by using a 'filled' wax sourced from Blayson Olefines Ltd, UK.Injection of molten wax was carried out using the above die and a 12 Ton wax injection machine was utilized for this purpose. Prior to injection, a die-release agent (silicone oil) was applied on the cavity walls for easy ejection of the pattern from the cavity. Initially, several trials were conducted to optimise the injection parameters such as injection temperature, injection pressure and dwell time. Such optimization of parameters was necessary to avoid defects such as fold, non-fill, chipping, distortions and cracks

Table 3. Optimised wax injection parameters used for making patterns.

Parameter	Value
Injection pressure (kg/cm^2)	20±2
Injection block temperature (°C)	70-75
Wax holding tank temperature (°C)	70-75
Die clamping pressure (kg/cm^2)	70±10
Suction time (s)	10±2
Dwell time (s)	90±10

in the pattern[9]. The optimized parameters used for injection are mentioned in Table 3. Apart from the patterns for the component, the same for test bars (13 mm diameter x 115 mm long rods needed for producing tensile and stress rupture samples) were also produced in a similar manner.

A wax 'cluster' was then prepared by assembling multiple component patterns along with the patterns of other essential parts, which include pouring cup, sprue rods, risers, cover plate, vent rods and gates. Joining of various wax parts to make a cluster was carried out by using a solder iron and the subsequent finishing of the joint regions by a special knife. The latter constituents of the cluster (i.e. pouring cup, sprue rods etc.) have simple shapes and are dimensionally non-critical. Therefore, they were prepared using an 'unfilled' wax sourced from the same supplier mentioned previously. To prepare them, molten unfilled wax was poured into the respective aluminium dies and allowed to solidify. The solidified pouring cup, sprue rods etc. were then joined with component wax patterns to make the required clusters. Each cluster contained 96 component patterns, as shown in Fig. 5(a).All the wax clusters were washed in a liquid solution containing trichloroethylene and isopropyl alcohol in distilled water (volume ratio: 1:1:80) to remove oil/grease from the surface. Subsequently, the clusters were washed thoroughly in distilled water and dried for about 15 h in a controlled environment maintained at a temperature of 20±2°C and relative humidity (RH) of 50±5%. Wax clusters of the test bars were also made in a similar manner (Fig.5 (b))[10].

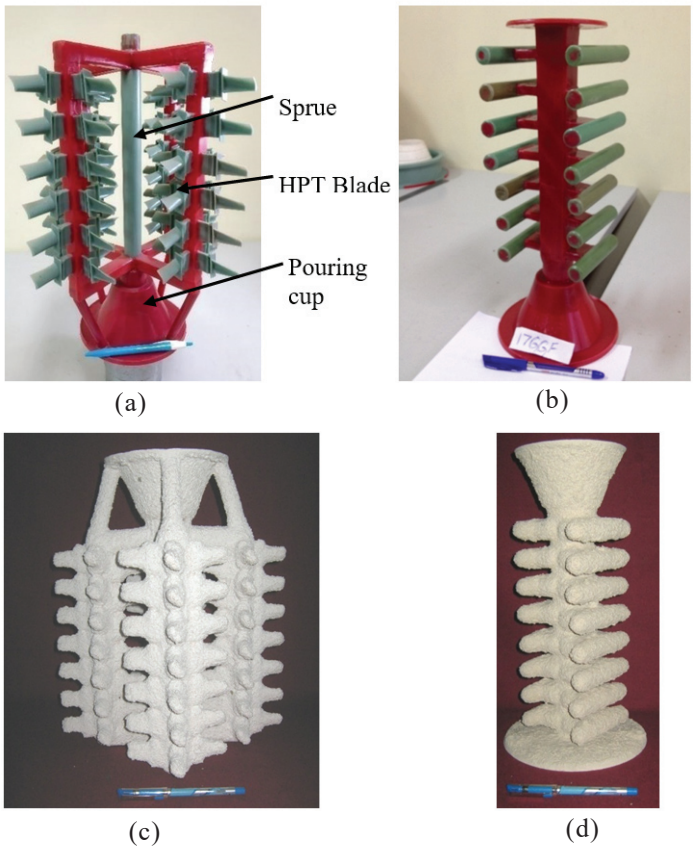

Figure 5. Typical wax clusters used in this study: (a) blades and (b) test bars. The corresponding ceramic moulds are shown in Fig. 5(c) and (d), respectively.

Ceramic moulds (or shells) required for casting operation is typically prepared by applying several layers of ceramic coating in the form of water-based slurry on wax clusters. The water-based slurry used in the present case consisted of a ceramic filler, a binder, a wetting agent, an anti-foaming agent and a nucleating agent in the required proportions. The quality of the slurry coats is the primary factor that determines the mechanical strength of the eventual ceramic shell. Factors such as size, size distribution and shape of particles in the filler material affect important properties of the slurry such as its viscosity which in turn affect the permeability and strength of the eventual shell mould[10]. Zircon was used as the filler material and colloidal silica, which is typically a colloidal dispersion of spherical silica particles in water, as binder. The slurry constituents were mixed inside a slowly rotating (18-20 rpm) stainless steel drum having a fixed agitation rod at the center. The drum was rotated till the slurry achieved a constant viscosity. The slurry was stirred throughout the shell-making process to prevent settling of powder particles. The viscosity was measured once every two hours using a Zahn cup 4 until the slurry became homogeneous with a constant viscosity. The density of the slurry was also measured along with its viscosity in the same time intervals. The details of the above measurements have been provided in our earlier publications[10-11].

Each wax cluster was repeatedly immersed in the slurry. After each immersion, it was taken out and placed in a rainfall sander where a stream of stucco particles fell from an overhead bin. These particles stuck on the wet slurry surface and gradually built the thickness of the ceramic layer. The stucco particles were so chosen that they effectively anchored the successive layers together. The first layer stucco material was about -100 mesh in size. The particle size of stucco was gradually increased for each successive coat and was about 1-1.5 mm for the final coat. While zircon sand was used as the stucco material for the first slurry coat, mullite grits were used for stuccoing 'after' the subsequent coats to achieve desired shell thickness, strength and refractoriness.After each stucco coating, the coated wax cluster was dried for 2-3 h in a controlled atmosphere room where temperature was maintained at 20±5°C and relative humidity at 15±5%. After the final stucco coat, the coated cluster was subjected to deep drying for about 20 h in the above mentioned room[11].

De-waxing (wax removal) of the dried ceramic shells was carried out in an autoclave (LBBC, UK make). Removal of wax from the ceramic shells occurs by melting the wax by a superheated steam at pressure of 100 psi inside the autoclave and allowing it (molten wax) to flow away under gravity into a collector box. The de-waxed moulds were fired in two steps in order to develop adequate strength in them through sintering as well as to remove the residual wax/volatiles/moisture. Moulds in the first step were heated in an air furnace at 550±20°C for about 1.5 h which was followed by cooling to room temperature (RT).Subsequently, they were subjected to 2nd step firing at 950±10°C for 1.5 h followed by cooling to RT in the same air furnace. These shells were subsequently used for casting of actual components (HPT blades and test bars). One mould each for HPT blades and test bars are shown in Fig.5(c) and (d), respectively.

3.2.2 Vacuum Melting and Casting

A vacuum induction melting furnace of 25 kg capacity (Consarc Inc., UK make) has been used for making castings of HPT blades and test bars. Initially, the mould was preheated to desired temperature and allowed to soak at that temperature for 2 h in the mould heating chamber. Subsequently, it was moved to the alloy melting chamber where the molten superalloy at 1540±10°C was poured into the mould. The molten metal was allowed to solidify and cool to RT inside the furnace. Pre-heating of mould and casting were carried out at a vacuum level of $1x10^{-3}$ Torr.

After cooling to room temperature, the ceramic mould was broken away by simple tapping/mild hitting. Subsequently, the required cast parts(blades/test bars) were separated from the clusters by cutting away the unnecessary parts using an abrasive cut-off machine and a wire EDM.Some of the cast parts are shown in Fig.6. These castings were subjected to various evaluations.

(a) (b)

Figure 6. Some of the cast parts: (a) blades and (b) test bars.

4. CHARACTERIZATION AND EVALUATION OF PROPERTIES

4.1 Non-Destructive Evaluation (NDE) of Components

All cast HPT blades underwent several non-destructive tests which include (a) visual examination, (b) macro-grain observation, (c) fluorescent penetrant (dye) inspection (FPI) and (d) X-ray radiography. NDE was carried out to detect surface and sub-surface defects, if any, present in the components. If the detected defects did not meet the acceptance criteria, the corresponding component was rejected. Prior to NDE, the components were sand blasted with alumina grit to clean the entire surface and also to remove oxide scale sticking to the surface. Visual inspection was carried out to identify the presence of dents/pits on its surface. Components having pits above a certain size (diameter of 0.7 mm and depth of 0.5 mm) were rejected. Accepted components were then subjected to macro-grain size observation on the surface. This was done after etching the parts in a solution of HCl (750 ml), HNO_3 (20ml), ferric chloride (150 g) and water (100ml). By and large, the macro-grain size in all the blade castings met the user requirement, i.e. the maximum acceptable grain size of 5mm, and there was no rejection of components at this stage.

Fluorescent Penetrant Inspection (FPI) of the cast parts was conducted in accordance with ASTM E1209 standard. The components were soaked in an oil-based fluorescent dye and subsequently washing them with water to remove the excess dye. The components were then dipped in an aqueous developer and dried. They were then viewed under ultra violet (UV) light to detect surface cracks and pores. The components having these defects were rejected and remaining ones subjected to evaluation by X-ray radiography (ASTME1742) for identification of sub-surface defects. An X-ray radiography unit of a 450 kV capacity (Xylon make, Model: 452) was used for the purpose. The radiography data of all the components were compared against the acceptance criteria. The ones not meeting the criteria were rejected and remaining components were subjected to dimensional inspection.

4.2 Measurement of Component Dimensions

All the blades that were found acceptable after NDE were inspected for their dimensions at various locations. For aerofoil components such as HPT blades, meeting the dimensional requirements is very important for their application in the actual engine. For the present blade, dimensions were measured along AB, AC and AD sections. The dimensions of each blade were measured by using the same 3-axis tactile CMM mentioned earlier. The investment cast parts, being near-net shape, inherently do not have any planar–reference surface. Therefore, aligning them with respect to the stacking axis is a challenging task. For this alignment, a reference point system, called 3-2-1 scheme, involving six points on the casting and an iterative convergence algorithm is adopted. This is a standard method for precision dimensional inspection wherein each critical location/section is scanned with a touch CMM probe and the measured dimensions compared against the nominal dimensions, i.e. dimensions given in the component drawing. Since the reference perpendicular planes were not available in case of the present HPT blade casting due to its design, its aerofoil was made to orient with the nominal CAD model using the above mentioned 3-2-1 referencing[14-15].

The CMM probe measured the coordinates of the six points and the deviations from the reference values were automatically recorded. The measurement iteration continued till the deviation error became less than a specified value (typically 5-10 µm). Subsequently, the aerofoil sections of the aligned casting were scanned and compared with the corresponding CAD model. The casting was dimensionally qualified if the errors in 'form', 'displacement' and 'rotation' of all three aerofoil sections were within the nominal values defined in Table 2.

4.3 Chemical Analysis and Cut-up Evaluation of Castings

Chemical analysis of the all the alloying elements (except C and S) was carried out using an inductively coupled plasma optical spectrometer (ICP-OES). C and S were analyzed by LECO CS-444. Analysis was carried out on three representative castings, one randomly chosen casting from three separate moulds (metal cluster) in accordance with ASTME354 standard. Cut-up evaluation of HPTB castings was carried out to estimate the level of micro-porosity in the castings. Six

representative castings, two each from three different moulds, were selected for this evaluation. Metallographic polishing of the components was carried out and the polished sections observed using an optical microscope. The amount of micro-porosity was measured by analyzing optical images taken from the as-polished samples by utilising commercially available image analysis software called Image.

4.4 Microstructural Characterization and Evaluation of Mechanical Properties

Measurement of hardness, tensile and stress rupture properties on separately cast rods (test bars) in heat treated condition was carried out. As mentioned previously, test bars were cast using the same parameters adopted for casting the components. These bars were given the required two-step solutionizing treatment (1210 °C/1 h followed by 1220 °C/1 h followed by gas fan quenching (GFQ) with Ar gas). Subsequently, a two-step aging treatment (1080 °C/4 h/GFQ followed by 870 °C/20 h/GFQ) was given Evaluation of the above properties was carried out as a part of user requirement. Both solutionizing and aging treatments were carried out in a vacuum heat treatment furnace at a vacuum level of 10^{-4} mbar[15].

For observing the microstructure of the alloy, samples were polished using standard metallography procedures. Some of the polished samples were etched using an etchant consisting of 45 ml HCl, 30 ml HNO_3 and 30 ml CH_3COOH.This etchant selectively dissolves γ' phase present in the microstructure. Observations were carried out using both optical microscope and scanning electron microscope (SEM).

Vickers hardness of the alloy was measured using a load of 20 Kg. Tensile tests were carried out at Room Temperature (RT) and 760 °C using a Walter Bai Universal Testing Machinewith a cross head speed of 1 mm/min, as per ASTM E8 and ASTM E21standard. Stress rupture properties were evaluated using a lever arm creep testing machine operated at a constant load in ambient atmosphere. The tests were carried out at a temperature-stress combination of 975°C/196 MPa. Two tests were carried out under each condition.

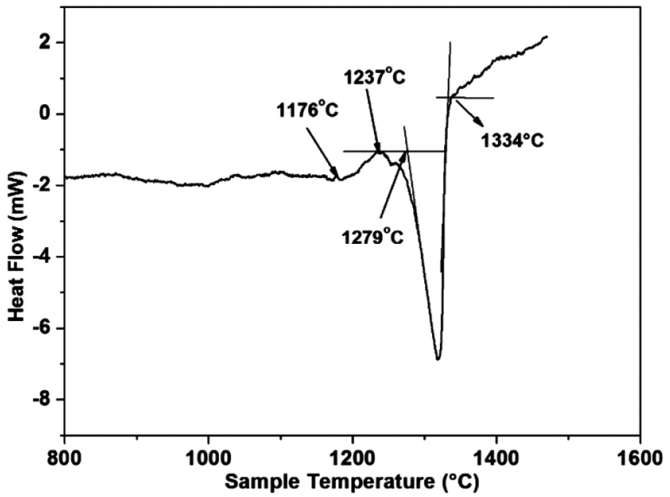

Figure 7. DSC plot for casting material indicating temperatures corresponding to γ' dissolution (1176°C), incipient melting (1237°C), solidus (1279°C) and liquidus (1334°C).

5. RESULTS AND DISCUSSION

5.1 Die-Related Aspects

As previously mentioned the HPT blade considered in this study is quite small and has a highly twisted design. In case of such small geometries having fine features, the ejection of wax pattern from the die after wax injection process is usually difficult as the pattern tends to stick to the movable die and this may result in pattern breakage. The deliberate addition of a 'T'-shaped projection to the firtree portion (Fig.5 (b)) not only helped retaining the wax pattern in the stationary half of the die but also aided in its easy removal from the die cavity. High surface finish of the cavity walls was also beneficial in avoiding the sticking of the patterns to the cavity walls and their possible damage. The fabricated dies for injection of wax patterns met all the dimensional requirements.

5.2 Ceramic Shell Making and Casting Related Aspects

The primary ceramic materials that were utilized for preparation of moulds, i.e. zircon filler, colloidal silica binder and mullite stucco, are typically used for most equiaxed and directionally solidified (DS) Ni-base superalloy parts of gas turbine engines. The moulds made from these constituents using the slurry coating method described above were able to withstand the high liquid metal temperature (1550°C) and metallostatic pressure. No bulging/sagging of the ceramic mould under this pressure and the consequent dimensional deviation was observed in the cast parts, as indicated from dimensional measurements described later (Fig. 11). Addition of a small amount of nucleating agent, i.e., cobalt aluminate, in shell material helped achieving a fine-grained equiaxed structure in the components. Several casting trials were also taken in order to standardize the casting parameters. The melt pouring temperature was decided based on the liquidus temperature of the present superalloy, which is 1334 °C, as determined from differential scanning calorimetry (DSC) analysis (Fig. 7). The metal pouring temperature was set at 1540±10°C which included a superheat of about 200 °C. Maintaining this superheat ensured that liquid metal had adequate fluidity to fill narrow crevices in the mould corresponding to thin trailing edges of the component.

To arrive at the right mould pre-heating temperature-time schedule, three different temperatures, namely 1080, 1120 and 1190°C were considered with duration of heating kept at 2 h in each case. The choice of above temperature/heating duration was based on our prior experience with Ni based superalloy castings Based on these trials,1190°C/2 h was found to be the most suitable preheating schedule for the moulds and was subsequently used for all the castings. This schedule was able to produce the required grain size in the components (0.5-5.0 mm). Lower mould preheating temperatures (such as 1080 and 1120°C) were found to produce unacceptably low grain sizes of <0.5 mm in the trailing edge region of the component[12-13].

Various types of casting-related defects were observed in the present components. Most frequently found defect includes inclusions and pore-clusters. The major cause for inclusion defects could be dislodgement of particles/chunks

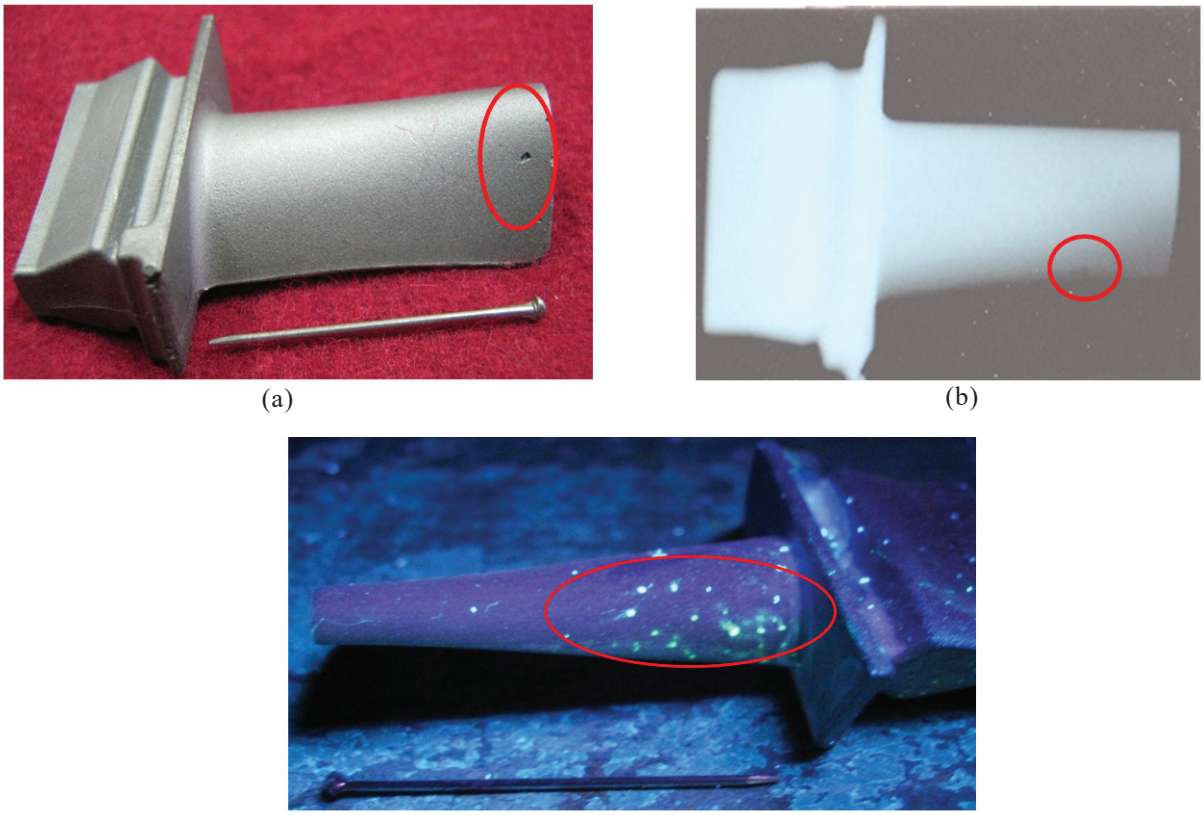

(a) (b) (c)

Figure 8. Typical defects observed in HPT blade castings: (a) surface depression caused by dislodgement of embedded inclusion, (b) sub-surface inclusion as revealed by radiography and (c) a cluster of porosity as revealed by FPI.

Table 4. Chemical analysis of randomly chosen three representative castings

Element	Specified (wt %)		Measured (wt %)		
	Min.	Max.	Blade-1	Blade-2	Blade-3
Cr	8.5	10.5	8.6	9.7	8.9
Co	12.0	15.0	13.5	15.2	14.1
W	1.0	1.8	1.29	1.4	1.27
Mo	2.7	3.4	2.98	3.30	3.30
Nb	0.5	1.0	0.74	0.79	0.68
V	0.5	1.0	0.81	0.92	0.84
Al	5.0	5.7	5.42	5.7	5.5
Ti	4.2	4.7	4.40	4.9	4.5
Zr	--	0.02	0.015	0.023	0.019
B	--	0.015	<0.01	<0.01	<0.01
Ce	--	0.02	<0.01	<0.005	<0.01
Si	--	0.4	0.1	0.085	0.091
Mn	--	0.4	<0.01	<0.00	<0.005
Fe	--	2.0	0.14	0.11	0.10
C	0.14	0.20	0.13	0.17	0.16
S	--	0.015	0.007	0.006	0.006
Ni	Balance		Balance	Balance	Balance

from the ceramic mould wall or graphite crucible (used for melting the alloy) and their embedment in the casting during solidification. Inclusions may be present on the surface or inside the component. Surface inclusions often get dislodged leaving behind a pit or depression. Occasional clusters of surface pores were also detected in FPI which had formed due to localized congregation of a few individual shrinkage pores during solidification. Components having the presence of any of the above defects beyond the specified acceptable limit were rejected. Figures 8(a)-(c) show some of the observed defects in the blade castings.

As previously mentioned, porosity levels at different locations of representative components were measured based on the cut-up inspection scheme (Fig. 9(a)). Porosities typically are caused by gas entrapment and/or by solidification shrinkage in the castings their formation in the Ni-base superalloys greatly depends on casting conditions as well as the chemical composition of the alloy. Presence of porosities in cast turbine blades beyond the specified levels is undesirable because they not only negatively affect the mechanical properties but also increase scatter in these properties. In all the inspected blades, the maximum level of porosity found was 0.8 vol. % against the specified limit of 1% in the aerofoil region and 2% in shank and root areas.

5.3 Aspects Related to Chemical Analysis, Microstructure, Mechanical Properties and Dimensions

Chemical composition of the superalloy in as-cast condition

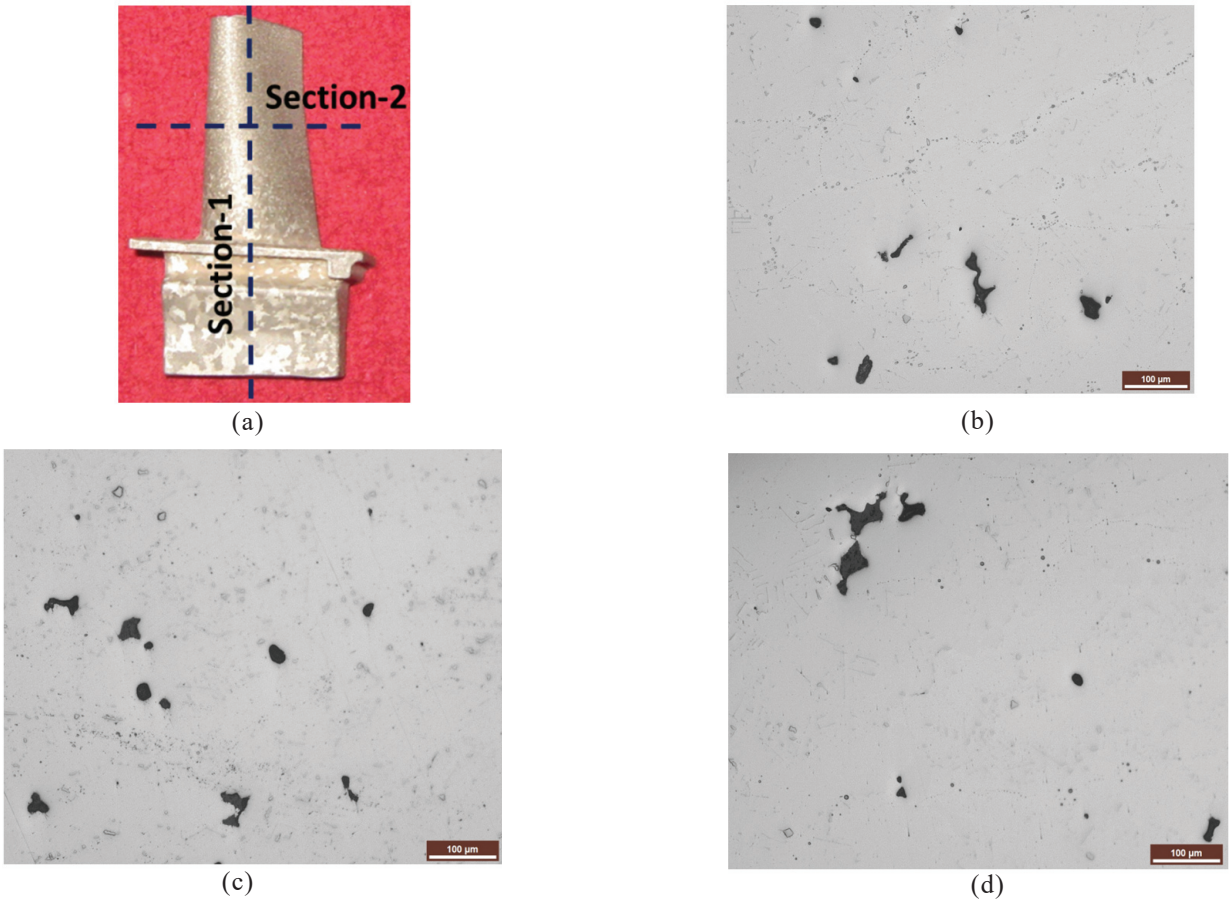

(a) (b) (c) (d)

Figure 9. Cut-up analysis of a typical HPT blade for porosity measurement: (a) cut-up scheme, (b) transverse section (section-2), (c) longitudinal section (section-1) in aerofoil region and (d) longitudinal section (section-1) in root region.

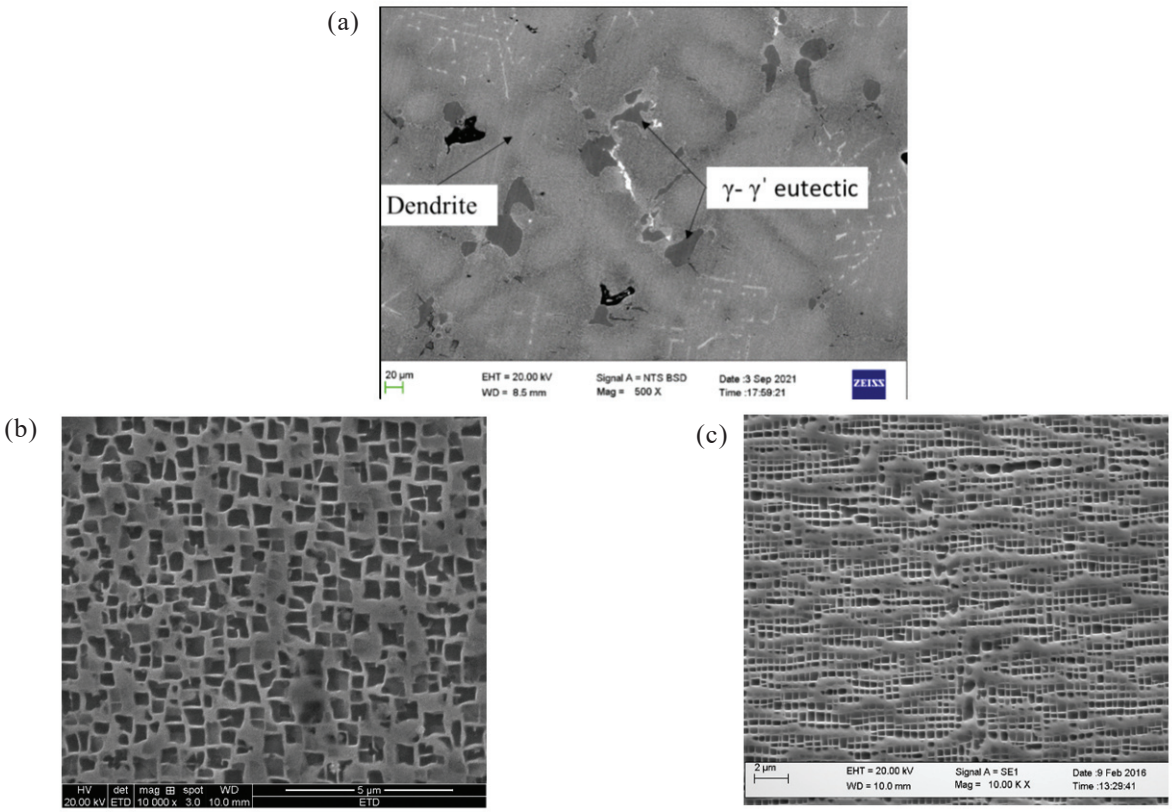

Figure 10. SE images of the microstructure of the alloy: (a) as-cast alloy showing dendritic and interdendritic regions, (b) γ-γ' structure in the dendritic regions of as-cast alloy and (c) γ–γ' structure in fully heat treated alloy.

Table 5. Maximum porosity levels (vol.%) measured at various locations in the three random HPT blades castings

Blade No.	Section (see Fig. 9(a))	Aerofoil region	Root and platform regions
1	1	1.01	1.15
	2	0.84	---
2	1	0.50	0.60
	2	1.00	---
3	1	0.22	< 2.00
	2	1.00	---

Table 6. Measured mechanical properties on test bars. Values mentioned in brackets are the minimum specified requirements

Tensile (solutionized + aged)			
		RT	760 °C
YS, MPa		761	835
UTS, MPa		830 (800)	899
% RA		10.4 (7.0)	9.5
Stress rupture (solutionized + aged, Tested at 975 °C/196 MPa)			
	Specified	Sample-1	Sample-2
Rupture life, h	40	66.2	88.7
% RA	-	9.0	9.0
Hardness (VHN)			
As-cast		Solutionized	Solutionized + Aged
352		363	363

with respect to the specified composition (i.e. with respect to the composition of the ingot which is remelted to cast the component) is important because any major deviation from the specified composition would indicate a potential degradation of mechanical properties of the component. Chemical analysis of the alloy done on three as-cast blades, as mentioned earlier, is provided in Table 4. As evident, the composition of the alloy did not undergo significant change due to casting operation and remained in the specified range. Figure 9(b)-(d) shows the typical porosity levels at various locations in the component in transverse and longitudinal sections (Fig. 9(a)). The porosity values for all the three representative components, as measured on both the sections at 100X magnification, are provided in Table 5. The porosity levels should be below the specified acceptable levels of 1 vol.% in aerofoil region and 2 vol.% in shank and root regions.

A typical optical micrograph of the as-cast structure in etched condition is shown in Fig. 10(a). The measurement for the amount of eutectic phase present was carried out on optical micrographs taken at a magnification of 100X. The volume percentage of eutectic in as-cast condition was measured to be about 5.5. Segregation of elements between dendrites and interdendritic regions can be clearly seen in the SEM BSE image of the as-cast microstructure (Fig. 10(a)).The eutectic phase, which was last to solidify, is present in the interdendritic region. The as-cast microstructure also revealed the secondary γ' phase in a matrix of γ in the intra-dendritic regions (Fig. 10(b)). However, this γ' phase had irregular shapes unlike the cuboidal shape observed after heat treatment (solutionizing and aging treatments) of the alloy[18]. After solutionizing treatment, the alloy revealed a significantly homogenized structure with volume percentage of the eutectic phase reducing to about 2.5%. The typical γ-γ' structure consisting of cuboidal secondaryγ' precipitates distributed in a γ matrix developed after the aging treatment, as seen in Fig. 10(c). The volume fraction of γ' precipitates in the above structure was about 0.5 and their size (measured as the diagonal length of the precipitates) 0.4-0.5 μm.

As previously mentioned, tensile and stress rupture properties were evaluated on heat treated test bars. Table 6 provides the measured hardness, tensile and creep properties of the alloy. As evident, both tensile and stress rupture properties of the cast bars met the specified property requirements for the use of the components. For example, the ultimate tensile strength (UTS) at room temperature (RT) was 830 MPa against the specified requirement of 800 MPa. The corresponding reduction in area (RA) was measured to be about 10% against the requirement of 7%. Similarly, a stress rupture life well above specified 40 h was achieved for the given heat treatment conditions.

Figure 11 shows the CAD model along with the CMM-measured dimensional profiles corresponding to three aerofoil cross-sections (AB, AC and AD, as shown in Fig. 2(a)) of a typical blade. The user-specified nominal profile and tolerance band (±0.13 mm) are also shown in Fig. 11(b)-(d). It is clear that the casting profile for any particular section (shown in red) is well within the tolerance band (shown in green) and is also very close to the nominal profile (shown in blue).

Table 7 provides the yield of cast HPT blades after each processing stage. A total of 1728 castings were made out of which 1286 were finally accepted which provides a casting yield of 74%. As evident, most of the rejections (about 25%) occurred after visual observations and FPI characterization. The final casting yield of 74 % of aeronautical-grade components such as HPT blade is fairly good and comparable with industrial yield values for complex Ni-base superalloy components such as the present HPT blade[6].

6. CONCLSIONS

The present paper provides details of vacuum investment casting method (established at DMRL) for manufacturing HPT blades that are used in the hot sections of an indigenously developed small turbo-fan engine. A commercially available Ni-base superalloy has been used for realizing the cast parts. Details pertaining to various steps of the casting process including design and fabrication of dies/tooling for wax patterns, wax pattern injection process, ceramic shell mould preparation, casting operation, non-destructive evaluation, measurement of dimensions, microstructural characterization and evaluation of mechanical properties have been provided. The required microstructural requirements in terms of level of porosity and microstructure have been met in the castings. The required tensile and stress rupture properties have also been achieved for the alloy in fully heat treated condition.

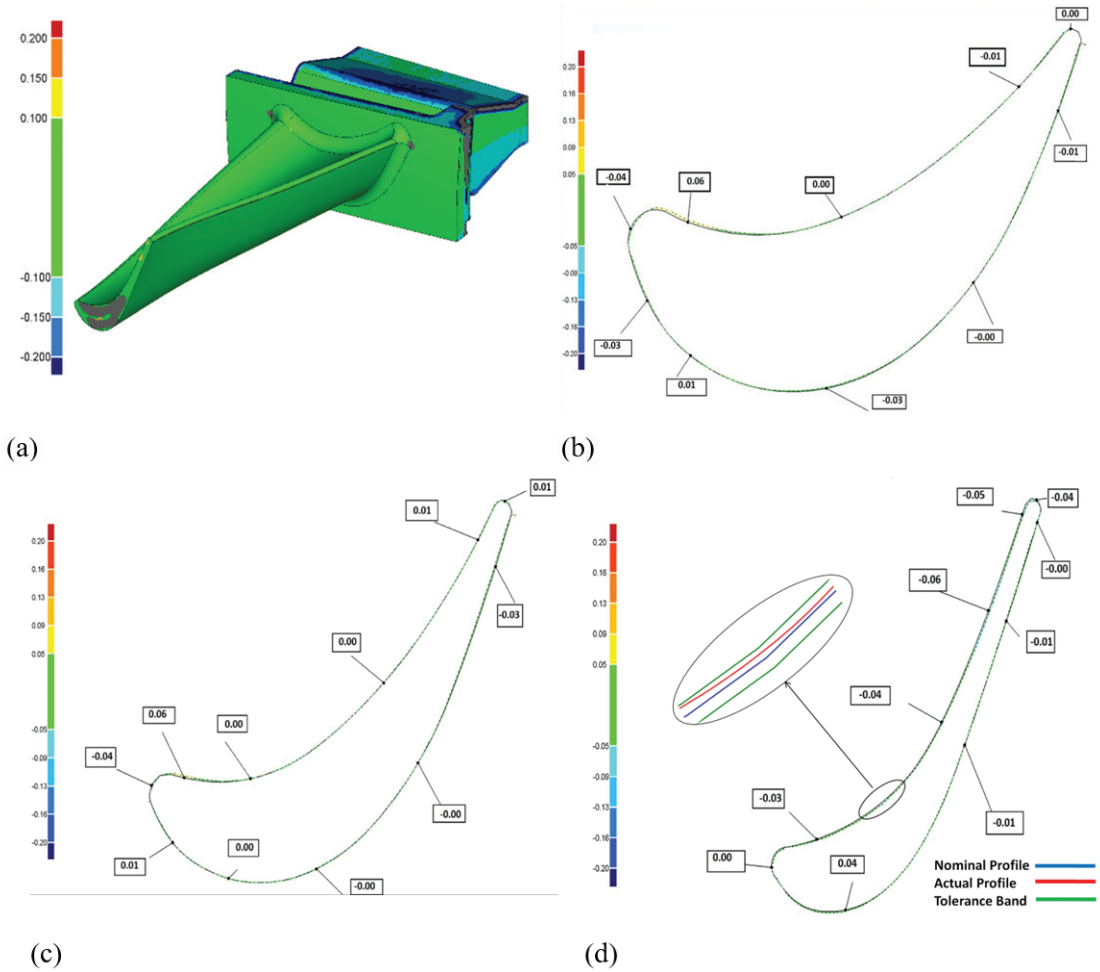

Figure 11. Laser CMM inspection results on a wax pattern injected using the manufactured die.(a) 3D best fit wax pattern and dimensional deviation values (in mm) in aerofoil section and corresponding 2D sections (b) AB; (c) AC and (d) AD (see Fig. 3(a)). The magnified inset in Fig. 11(d) clearly shows the actual profile (in red) with respect to the tolerance band (in green) and nominal profile (in blue). The deviations at various locations are mentioned in boxes.

Table 7. Casting yield after each processing step (a total of 1728 castings prepared for realizing 1286 components that were supplied)

Step	Nos. rejected	Nos. accepted	Yield (%)
Visual inspection	204	1524	88
FPI	226	1298	75
Radiography	12	1286	74
Dimensions	0	1286	74
Final casting yield for the component			74

Based on the production of nearly 1700 cast components, the casting yield achieved was about 74%, which is comparable to values available from industrial manufacturers of complex aeronautical-grade cast Ni-base superalloy parts.

REFERENCES

1. Reed, R.C. The superalloys: Fundamentals and applications, Cambridge University Press, 2008. doi: 10.1017/CBO9780511541285
2. Sims, C.T.; Stoloff, N.S. & Hagel, W.C. Superalloys II: High temperature materials for aerospace and industrial power. John Wiley and Sons, New York, 1987.
3. Onyszko, A.; Kubiak, K. & Sieniawski, J. Turbine blades of the single crystal nickel based CMSX-6 superalloy. *J. Achiev. Mater. Manuf. Eng.*, 2009, **32**, 66-69.
4. Pollock, T.M. & Tin, S. Nickel-based superalloys for advanced turbine engines: Chemistry, microstructure, and properties. *J. Propulsion and Power*, 2006, **22**, 361-374. doi: 10.2514/1.18239
5. Kanyo Janos, E.; Schafföner, Stefan; Uwanyuze R, Sharon; & Leary Kaitlynn, S. "An overview of ceramic molds for investment casting of nickel superalloys", *J. Eu. Ceram. Soc.*, 2020, **40**(15), 4955-4973. doi: 10.1016/j.jeurceramsoc.2020.07.013
6. Sriramamurthy, A.M. Investment casting: A treasure trove. DRDO Monographs/Special Publications Series, ISBN 978-81-86514-83-2, 2015.
7. Thakre, Prashant; Chauhan, Alok Singh; Satyanarayana, A.; Kumar, E. Raj & Pradyumna, R. "Estimation of shrinkage & distortion in wax injection using Moldex3D simulation", Materials today: Proceedings, 2018, **5**(9), 19410-19417 doi: 10.1016/j.matpr.2018.06.301
8. Pattnaik, Sarojrani; Karunakar, D.B. & Jha, P.K. "Influence of injection process parameters on dimensional stability of

wax patterns made by the lost wax process using taguchi approach", Proceedings of the Institution of Mechanical Engineers, Part L, *J. Mater.: Design Appl.*, 2013, **227**(1), 52–60.
doi: 10.1177/1464420712451807

9. Atlas of wax pattern defects. Investment Casting Institute, Montvale, NJ 07645-1720, www.investmentcasting.org. (Accessed on 20 October 2022).
10. Venkat, Y.; Choudary, K.R.; Das, D.K.; Pandey, A.K. & Singh, Sarabjit, "Ceramic shell moulds with zircon filler and colloidal silica binder for investment casting of shrouded low-pressure turbine blades", *Ceramics Int.*, 2020, **46**(17), 26572-26580.
doi: 10.1016/j.ceramint.2020.07.125
11. Venkat, Rao T.S.; Saurabh, K.; Chatterjee, D.; Hazari, N.; Singh, S. & Das, N. Optimization of mullite shell mould for casting of advanced nickel-base superalloys, DMRL Technical Report: DRDO-DMRL-DSG-092-2015, 2015.
12. Raza, Mohsin. Process development for investment casting of thin-walled components. Malardalen University Press, Sweden, Thesis no. 199, 107-121, 2015.
13. Reed, R.C. & Rae, C.M.F. Physical Metallurgy of the Nickel-Based Superalloys. Physical Metallurgy. Fifth Edit., Elsevier, 2215-2290, 2014
doi: 10.1016/B978-0-444-53770-6.00022-8
14. Zhang, D.; Cheng, Yunyong; Jiang, Ruisong & Wan, Neng. Turbine blade investment casting die technology. National Defence Industry Press and Springer-Verlag GmbH Germany, 2017.
doi: 10.1007/978-3-662-54188-3
15. Bosch, J.A. Coordinate measuring machines and systems. Marcel Dekker Inc., 1995. ISBN 0824795814 (ISBN13: 9780824795818)
16. Safari, J. & Nategh, S. On the heat treatment of Rene-80 nickel-base superalloy. *J. Mater. Processing Technol.,* 2006*,* **176**(1-3), 240–250.
doi: 10.1016/j.jmatprotec.2006.03.165.
17. Chatterjee, D.; Hazari, N.; Das, N. & Mitra, R. Microstructure and creep behavior of DMS4-Type nickel based superalloy single crystals with orientations near <0 0 1> and <011>. *Mater. Sci. Eng. A*, 2010, **528**(2), 604–13.
doi: 10.1016/j.msea.2010.09.083
18. Chen, C.; Sun, J.; Diao, A.; Yang, Y.; Li, J. & Zhou, Y. On the dendrite deformation and evolution mechanism of Ni-based superalloy during directional solidification. *J. Alloys Compd.*, 2021, **891**,161949, 2022,
doi: 10.1016/j.jallcom.2021.161949.

CONTRIBUTORS

Mr Dibyendu Chatterjee obtained MTech. from IIT, Kharagpur, and working as Scientist at DRDO-DMRL, Hyderabad. His area of research includes development and production of single crystal turbine aerofoil components.
His contribution in current study is experimentation, test results, analysis

Mr Alok Singh Chauhan obtained his MTech (Mechanical Engineering) from IIT, Bombay and working as Scientist at DRDO-DMRL, Hyderabad. His areas of interests are tool design and manufacturing of for investment cast components of aero engine gas turbine, CNC milling, Electro-Discharge machining, machining of aero engine castings made of nickel based single crystal superalloys, 3D printing and Finite element analysis.
His contribution to the current study includes design, manufacturing and result analysis

Mr Venkat obtained his BE (Ceramic and Cement Technology) from Gulbarga University, Gulbarga and working as Scientist at DRDO-DMRL, Hyderabad. His main field of work is development and production of ceramic shell moulds for investment castings of gas turbine components using nickel-base superalloys including characterization of raw materials used for shell moulds. He has developed mullite and alumina shell mould system for investment casting of gas turbine DS and SX components using advanced nickel base superalloys.
In current study, he has provided valuable input in experimentation.

Ms D.P. Tigga obtained her BTech in metallurgical and materials engineering from IIT, Kharagpur and working as Scientist at DRDO-GTRE, Bengaluru. Her area of research includes characterisation of investment casted nickel based superalloys used for gas turbine engine components.
In the current study she has contributed in material characterization.

Dr D.K. Das is working as Senior scientist at DRDO-DMRL, Hyderabad. His areas of specialization are superalloy castings and high temperature coatings for gas turbine engine applications, coatings for missiles and hypersonic vehicles, laser material processing and plasma particle interaction.
His contribution includes conceptualization, methodology, review and editing the manuscript.